Scholar Commons
USF University of South Florida

University of South Florida
Scholar Commons

Graduate Theses and Dissertations | Graduate School

June 2018

Expediting the Consolidation of Clayey Soils Utilizing Microwaves

Thilini Jayatissa
University of South Florida, thilini.jay157@gmail.com

Follow this and additional works at: https://scholarcommons.usf.edu/etd

 Part of the Other Civil and Environmental Engineering Commons

Scholar Commons Citation
Jayatissa, Thilini, "Expediting the Consolidation of Clayey Soils Utilizing Microwaves" (2018). *Graduate Theses and Dissertations.*
https://scholarcommons.usf.edu/etd/7310

This Thesis is brought to you for free and open access by the Graduate School at Scholar Commons. It has been accepted for inclusion in Graduate Theses and Dissertations by an authorized administrator of Scholar Commons. For more information, please contact scholarcommons@usf.edu.

Expediting the Consolidation of Clayey Soils Utilizing Microwaves

by

Thilini Jayatissa

A thesis submitted in partial fulfillment
of the requirements for the degree of
Master of Science in Civil Engineering
Department of Civil and Environment Engineering
College of Engineering
University of South Florida

Major Professor: M. Gunaratne, Ph.D.
M. Celestin, Ph.D.
A.Tejada-Martinez, Ph.D.

Date of Approval:
June 19, 2018

Keywords: Settlement, Thermal, Irradiation, Hydaulic Conductivity, Kaolin

Copyright © 2018, Thilini Jayatissa

DEDICATION

I dedicate this work to my family and friends for their relentless support and encouragement toward my educational accomplishments.

ACKNOWLEDGMENTS

I am grateful to my major professor, Dr. M. Gunaratne, for giving me the opportunity to work on this project. I am very appreciative for his support throughout this journey. I also appreciate the numerous support and encouragement I received from the research engineers at the College of Engineering, Dr. M. Celestin and Mr. Mike Konrad. My special thanks is extended to Dr. Gray Mullins for his support in practical implementations. I thank Mr. Chuck McGee at the College of Arts, ceramics department for sharing his knowledge of practical experimentation. I am thankful to all my colleagues at the Department of Civil Engineering for their support.

TABLE OF CONTENTS

LIST OF TABLES

LIST OF FIGURES

ABSTRACT

Post-construction settlement has been an issue in the field of construction due to the excessive time taken for the dissipation of pore water pressure. This is significant for construction carried out on clayey soils primarily due to the low permeability of clayey soils. Therefore, attention has been directed at finding means of increasing the rate of pre-consolidation. Recent research has focused on the effects of temperature on consolidation. It has been shown that elevated temperature increases the hydraulic conductivity of pore water due to both the reduction of viscosity and differential volumetric expansion of soil and water. This results in an increase in the rate of pore pressure dissipation. In addition, it has been proven that compressibility properties also improved at elevated temperature and subsequently, the rate of consolidation of the clay.

This research aimed to study the feasibility of utilizing microwaves to expedite the aforementioned temperature elevation and the subsequent consolidation of a clay soil. A numerical model has been formulated using finite difference methods to theoretically predict the temperature rise and pore pressure dissipation. The results of the numerical model proved to be in general agreement with the experimental data. The feasibility of utilizing microwaves to raise the temperature of the soil sample was also evaluated practically by conducting bench-scale experiments. The use of microwave irradiation to rapidly increase the temperature of saturated clay was quantified by this research and was proven to be more efficient than currently used soil heating methodologies. Comparable consolidation experiments showed that increasing the

temperature of the sample using microwave heating resulted in a higher rate of settlement when compared with the settlement of the non-heated sample while the ultimate percentage settlement of both were equal.

CHAPTER 1: INTRODUCTION

1.1 Effect of Temperature on Rate of Settlement

1.1.1 Increase in Hydraulic Conductivity

Hydraulic conductivity refers to the ease with which water can flow through porous media and can be expressed as in equation (1),

$$k = K\frac{\gamma}{\mu} \tag{1}$$

where, k is the hydraulic conductivity, K is the intrinsic hydraulic conductivity (or permeability), γ is the unit weight of water and μ is the viscosity of water.

Research by Abuel-Naga, Bergado, & Chaiprakaikeow (2006) indicates an increase in hydraulic conductivity with increasing temperature. This corresponds to a decrease in viscosity of water

1.1.2 Generation of Excess Pore Water Pressure

Clay consolidation process is driven entirely by an applied surcharge. The increase in overburden stress will generate an excess pore pressure. However, pore pressure can be further increased by increasing the temperature of the clay. This phenomenon can be attributed to the difference of the coefficient thermal expansion (CTE) between clay skeleton and water. In

comparison with the clay skeleton, water has a significantly higher CTE. Therefore, a clay sample, when heated, would generate excess pore water pressure due to differential volumetric expansion.

For a dry soil skeleton, the relevant analytical representation is as follows. Considering the initial volume of voids (Vo) , thermal expansion coefficient of the soil skeleton (α_{soil}), temperature increase (ΔT), the final volume of voids (Vv) can be written as:

$$V_v = V_o(1 + \alpha_{soil})\Delta T \tag{2}$$

For a saturated sample, the initial volume of water can be equated to V_o. Then the final volume of water V_w can be written as,

$$V_w = V_o(1 + \alpha_{water})\Delta T \tag{3}$$

Therefore, the differential volumetric expansion can be written as:

$$\Delta V = Vw - Vv = Vo(\alpha_{water} - \alpha_{soil})\Delta T \tag{4}$$

However, the thermal expansion of water is far greater than that of the soil skeleton. Therefore, the differential volumetric expansion, and the subsequent pore pressure increase can be attributed mostly to the expansion of pore water. Hence, Eq (3) can be simplified to Eq (4).

$$\Delta V = Vw - Vv = Vo.\alpha_{water}.\Delta T \tag{5}$$

1.2 EM Irradiation of Soils

In recent years, there has been a shift of interest toward utilizing electro-magnetic (EM) waves to increase the temperature of soil. This interest is fueled by the ability of EM waves, microwaves (MW) in particular, which operate on principles of radiation, to rapidly heat the soil to higher temperatures. Current research has been more or less limited to utilizing MW irradiation

for soil remediation. Falciglia et al. in 2015 conducted lab scale experiments on diesel contaminated soils using 2.45GHz microwaves with an incident electric field of 1000 V/m for a period of 6 days and achieved temperatures higher than 180 ^{o}C. Thus, in pre-consolidation of clay, utilization of microwaves could prove to be a more effective heating alternative to conventional injection wells.

However, a significant limitation of using MW irradiation would be its high attenuation. The higher the frequency of incident EM wave the higher the attenuation. Falciglia (2016), used 2.56 GHz MW for soil decontamination and observed negligible thermal effects past a maximum distance of 0.2m. However, this limitation maybe overridden as the soil dielectric properties are temperature dependent. The increase in temperature was seen to change the dielectric properties and consequently increase the depth of penetration of the waves which resulted in a progressive increase in the electric field penetration into soil [7]. However, there is limited knowledge available in the literature on the variation of above parameters.

1.2.1 Heating Mechanism

The heating of water molecules under an applied EM field can be attributed to the polarity of water molecules. A high frequency alternating electric field applied on a dipolar molecule causes molecular dipole rotation whereby polar molecules continuously attempt to align themselves in an electric field. This leads to a dissipation of kinetic energy which is reflected by an increase in temperature. This phenomenon could be directly applied to the heating of saturated soil. During irradiation, the dipole pore water would react to the incident electric field thus heating the bulk soil.

1.2.2 Effects of Soil Moisture on Temperature Variation

The temperature variation of soil is greatly dependent upon the soil moisture content. Hallikainen et al. (1985) observed that dielectric constants of soil were roughly proportional to the water content of soil and decrease with electromagnetic wave frequency. Robinson et al (2012) observed that dielectric constant and loss factor of soil, and subsequently the absorption MW energy, were relatively high in soils at temperatures less than 100 ^{o}C. It was observed that above 100 ^{o}C, due to the loss of free water by evaporation, the soils became much less absorbent.

CHAPTER 2: NUMERICAL MODEL

2.1 Principles of MW Penetration in Soils

During soil irradiation, MW energy is partially absorbed and converted to heat in clay according to the law of Lambert and Beer. (Barba et al., 2012) This generates an exponential decrease of the local electric field (E) with the distance from the MW source (d) as Eq. (6),

$$E = E_0 . e^{-\frac{d}{D_p}} \tag{6}$$

where E_0- incident electric field (V/m) and D_p- penetration depth of MW. The penetration depth of MW for loss dielectric materials such as clay, can be calculated using Eq.(7),

$$D_p = \frac{\lambda_0}{2\pi} . \frac{\sqrt{\varepsilon'}}{\varepsilon''} \tag{7}$$

where λ_0 is the wavelength of the irradiation (m) whereas ε' and ε' are the real and imaginary part of the complex dielectric permittivity of the clay respectively. The electric power dissipated into a unit volume of clay is quantified by Eq. (8) which is derived using the Maxwell's equations (Metaxas and Meredith, 1993),

$$\dot{Q} = \frac{1}{2}\omega\varepsilon_0\varepsilon''|E^2{}_{max}| = \omega\varepsilon_0\varepsilon''|E^2| \tag{8}$$

where ω is the angular frequency, ε_0 is the permittivity of free space (8.85 x 10^{-12} F/m), E_{max} is the electromagnetic field peak value (V/m) and E is electromagnetic field effective value (V/m).

2.2 Governing Equations of Water and Heat Flow

Assuming that the source of MW irradiation (antenna) is installed at the center of the cylindrical sample and spans the entire depth of clay sample, the model can be considered axisymmetric about the vertical axis of the antenna (Fig. 2.1). The flow towards the top and bottom surfaces of the clay sample are restricted with the use of impervious barriers. Additionally, assuming a uniform irradiation zone, which results in a uniform temperature distribution in the vertical direction, the model can be simplified to a one-dimensional radial problem. The numerical models are derived for a finite element at a radial distance r from the heat source.

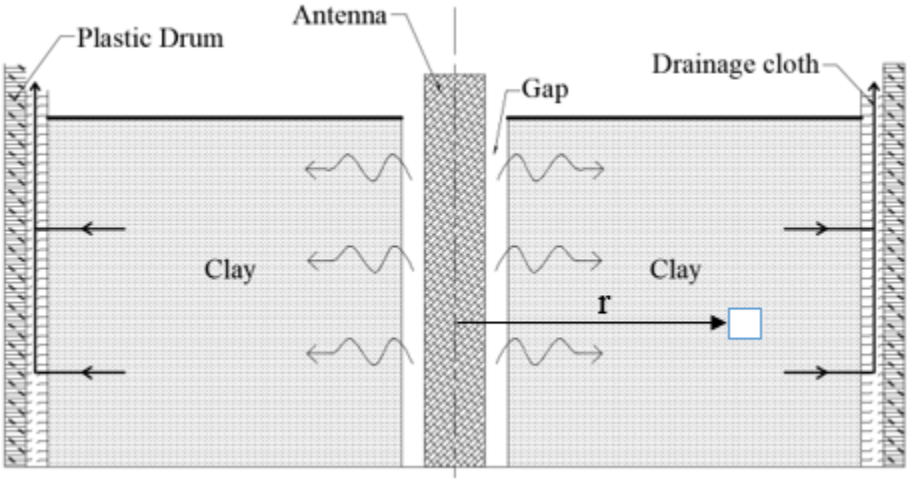

Figure 2.1 Finite element at a distance r from irradiation source considered for numerical model

2.2.1 Heat Transfer Equation

The rate of heat absorbed into a radial element at a distance r from the heat source will be the summation of the rates of heat conducted into the element and that generated by the applied EM field - $\dot{Q}$. This is expressed in Eq. (9),

$$n\rho_w c_w \left(\frac{\partial T}{\partial t}\right) + \rho_s c_s (1-n)\left(\frac{\partial T}{\partial t}\right) = \left(\frac{k}{r}\right)\nabla^2 T + \dot{Q} \tag{9}$$

where ρ_w, ρ_s, c_w, c_s are the density and specific heat capacity of water and soil (kaolin clay) respectively and n and k are the porosity and thermal conductivity of the clay respectively. Using Eq. (8) this can be rewritten as,

$$(n\rho_w c_w + \rho_s c_s (1-n))\frac{\partial T}{\partial t} = k\left[\frac{\partial^2 T}{\partial r^2} + \left(\frac{1}{r}\right)\frac{\partial T}{\partial r}\right] + \omega\epsilon_0\varepsilon'' E_0^2 . e^{-\frac{2r}{D_p}} \tag{10}$$

2.2.2 Equation of Water Flow

The rate of flow within a finite element can be derived using the Darcy's equation for water flow, the volumetric expansion of pore water due to temperature rise and the rate of pore volume change as,

$$0 = \frac{K_h}{\gamma_\omega}\left[r\frac{\partial^2 u}{\partial r^2} + \frac{\partial u}{\partial r}\right] + \frac{\partial n}{\partial t} + n\,\alpha_\omega\left[\frac{\partial T}{\partial t}\right] \tag{21}$$

where, K_h- horizontal hydraulic conductivity of clay, γ_ω- specific gravity of water, c-coefficient of compressibility, α_ω- thermal expansion coefficient of water and n- porosity.

2.2.3 Pore Pressure and Porosity Relation

The porosity and effective stress within a finite element of a saturated sample, for constant total stress, can be related as shown in Eq. (12) using fundamental soil theory.

$$d\sigma' = -\frac{\sigma'}{c(1-n)^2}.dn \tag{12}$$

where, σ' -effective stress acting on the element. However as, $d\sigma' = -du$, Eq (12) can be written as,

$$-du = -\frac{\sigma - u}{c(1-n)^2}.dn \tag{13}$$

Equations (10) (11) and (13) together governs the temperature variation and subsequent pore pressure dissipation of the system.

2.2.4 Boundary Conditions

A total of 6 boundary conditions (b.c.s) are needed to solve the above equations. It is assumed that, initially the pore pressure of the sample is equal to the stress increase due to the load on the sample. The sample is also assumed to be open to the atmosphere at the surface adjacent to the antenna and at the outer periphery of the sample. The temperature b.c. at the innermost boundary was imposed assuming a negligible thermal conductivity of the air contained in the small air gap between the sample and antenna. The entire sample is also assumed to be perfectly insulated while the heat conducted at the outer radius is assumed to be absorbed completely into the surrounding plastic container. The boundary conditions are summarized below.

1) Pore pressure boundary conditions (Note: all pressure values are gauge pressures):

   a) $u_{r,0} = P_1$, where P_1 is the stress increase in the clay sample caused by the added load.

   b) $u_{n,t} = 0$, circumferential end of the sample is open to the atmosphere

   c) $u_{1,t} = 0$, soil sample is not flush with the antenna and is open to the atmosphere

2) Temperature boundary conditions:

   a) $T_{r,0} = T_0$, where T_0 is the measured temperature at the beginning of the clay sample.

   b) $\left.\frac{\partial T}{\partial r}\right|_{1,t} = 0$, no temperature gradient at the inner boundary of the sample

   c) $-k\left.\frac{\partial T}{\partial r}\right|_{n,t} = m_p c_p \frac{\partial T}{\partial t}$, conduction at soil boundary is absorbed into the plastic container.

2.2.5 Finite Difference Approximations

The heat balance equation (10), flow equation (11) and compressibility equation (13) were simultaneously solved using the finite difference method based on forward time centered space scheme. Due to the axisymmetry of the soil sample and uniformity in the z direction, a radial axis at any elevation within the soil sample can be considered in a 1D model.

2.2.5.1 Finite Difference Form of the Heat Transfer Equation

The following finite difference form can be written for Eq. (10) for inner uniformly placed nodes with central difference in the special direction and forward difference in time.

$$(n\rho_w c_w + \rho_s c_s(1-n))\left[\frac{T_{r,t+1}-T_{r,t}}{\Delta t}\right] = k\left[\left(\frac{T_{r+1,t}-2T_{r,t}+T_{r-1,t}}{(\Delta r)^2}\right) + \left(\frac{1}{R}\right)\left(\frac{T_{r+1,t}-T_{r-1,t}}{2.\Delta r}\right)\right] + \omega\epsilon_0\varepsilon'' E_0^2.e^{-\frac{2r}{D_p}} \quad (14)$$

For unevenly spaced nodes with central difference method in the spatial direction and forward difference in time, the above equation modified to Eq. (15).

$$(n\rho_w c_w + \rho_s c_s(1-n))\left[\frac{T_{r,t+1}-T_{r,t}}{\Delta t}\right] = k\left[2\left(\frac{d_1.T_{r+1,t}-(d_1+d_2)T_{r,t}+d_2.T_{r-1,t}}{d_1 d_2(d_1+d_2)}\right) + \left(\frac{1}{r}\right)\left(\frac{d_1^2.T_{r+1,t}+(d_2^2-d_1^2)T_{r,t}-d_2^2.T_{r-1,t}}{d_1 d_2(d_1+d_2)}\right)\right] + \omega\epsilon_0\varepsilon'' E_0^2.e^{-\frac{2r}{D_p}} \quad (15)$$

2.2.5.2 Finite Difference Form of the Flow Equation

The flow equation (Eq. 11) can be rewritten for inner uniformly placed nodes with central difference in spatial direction and forward difference in time as follows.

$$0 = \frac{K_h}{\gamma_\omega}\left[r\left(\frac{u_{r+1,t} - 2u_{r,t} + u_{r-1,t}}{(\Delta r)^2}\right) + \left(\frac{u_{r+1,t} - u_{r-1,t}}{2.\Delta r}\right)\right] \quad (16)$$

$$+ \left(\frac{cR(1-n)^2}{\sigma'}\right)\left[\frac{u_{r,t+1} - u_{r,t}}{\Delta t}\right]$$

$$+ n\,\alpha_\omega\left[\frac{T_{r,t+1} - T_{r,t}}{\Delta t}\right]$$

For unevenly spaced nodes with central difference method in the spatial direction and forward difference in time, the above equation modified to Eq. (17).

$$(n\rho_w c_w + \rho_s c_s(1-n))\left[\frac{T_{r,t+1} - T_{r,t}}{\Delta t}\right] \quad (17)$$

$$= k\left[2\left(\frac{d_1 . T_{r+1,t} - (d_1 + d_2)T_{r,t} + d_2 . T_{r-1,t}}{d_1 d_2 (d_1 + d_2)}\right)\right.$$

$$\left. + \left(\frac{1}{r}\right)\left(\frac{d_1^2 . T_{r+1,t} + (d_2^2 - d_1^2)T_{r,t} - d_2^2 . T_{r-1,t}}{d_1 d_2 (d_1 + d_2)}\right)\right]$$

$$+ \omega\epsilon_0\varepsilon''\,E_0^2 . e^{-\frac{2r}{D_p}}$$

2.2.5.3 Finite Difference Form of the Porosity Equation

The porosity equation can be written for any node with forward difference in time as,

$$n_{r,t+1} = \left[\frac{(u_{r,t} - u_{r,t+1})}{\left(\frac{\sigma - u_{r,t}}{c(1-n_{r,t})^2}\right)}\right] + n_{r,t} \quad (18)$$

2.2.6 Computer Coding

As illustrated in Fig. 2.2, in the numerical model, a given radial axis was divided into segments of equal size and nodes were introduced at the center of each segment. The last node on the radial axis was considered to be representative of the plastic drum. The numerical grid consisted of 129 equally spaced grid points of Δd=0.001m radial spacing and the temporal spacing was optimized to achieve a minimum time step while ensuring stability of numerical model. The time step used was 0.05s

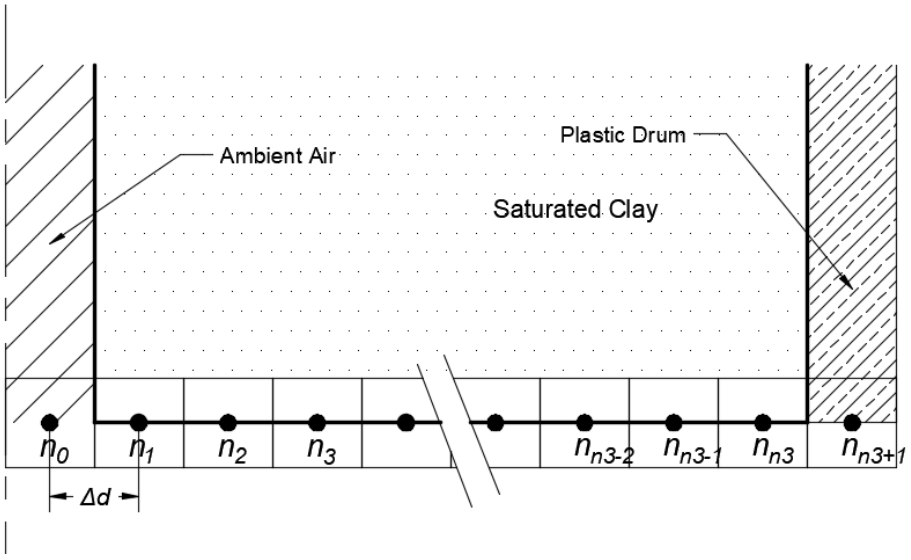

Figure 2.2 Grid point definition in the radial domain of the sample

Subsequently, the heat transfer equations (14 & 15), the flow equation (16 & 17) and porosity equation (18) were solved simultaneously in the numerical model.

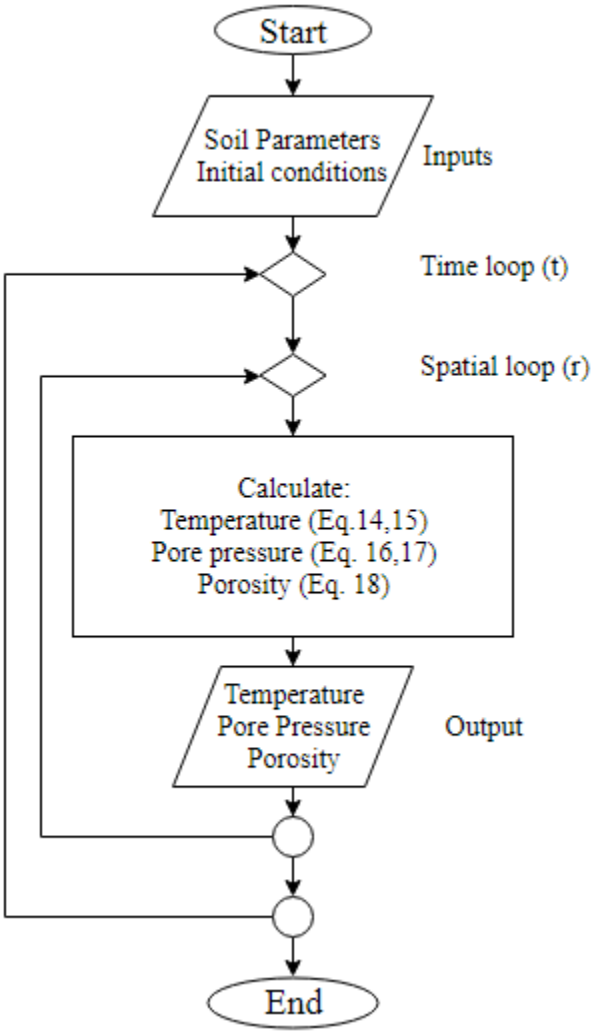

Figure 2.3 Flow chart for numerical model

2.2.6.1 Soil and MW Parameters

The parameters shown in Table 2.1 were used in the implementation of the program for radial consolidation based on MW heating. The initial temperature of the entire clay sample was assumed to be uniform at a value T_0=22.5 ºC.

Table 2.1 Soil and MW parameters

Description	Value	Units
Height of soil layer	0.11938	m
Specific heat capacity of water	4184	J/kg.K
Specific heat capacity of Kaolin	1010	J/kg.K
Specific heat capacity of plastic	1900	J/kg.K
Specific weight of clay	16000	N/m3
Specific weight of water	9810	N/m3
Density of dry kaolin	2650	kg/m3
Density of water	985	kg/m3
Density of plastic	950	kg/m3
Initial temperature of clay	22.5	ºC
Initial temperature of plastic	22.5	ºC
Annular frequency	5.65 x 106	rad/s
Dielectric permittivity of free space	8.8 x 10-6	F/m
Wavelength of MW	0.333	m
Thermal conductivity of kaolin clay	1.2	W/m.K
Coefficient of compressibility	0.3	m2/s
Hydraulic conductivity of clay	7.8 x 10-8	m/s
Initial porosity of the sample	0.5	

CHAPTER 3: EXPERIMENTAL SETUP

Two separate experiments were conducted during this research. The first experiment was conducted on a soil sample of an approximate volume of 4 gal with the primary objective of observing the spatial and temporal temperature variation of the sample caused by MW heating. The second experiment was conducted on two identical soil samples for a duration of 6 days. The objective of the latter experiment was to compare both the magnitude and rate settlement of the soil under identical loading conditions with and without MW heating.

3.1 Preparation of the Soil Sample

Two identical soil samples were prepared each by mixing 150 lb of dry EPK Kaolin clay powder, 80 lb of silica sand to create a 4:1 clay to sand dry mix. This was mixed with 43 lb of water to create saturated clay samples of specific weight 16 kN/m3.

Figure 3.1 Mixing of kaolin and sand to make the clay mix

Figure 3.2 Packing of clay mix into the plastic drum

3.2 Frequency Selection of the Microwaves

Of the wide range of electromagnetic waves (EMWs), microwaves (MW) can be classified as EMWs with frequencies in the range 300 MHz - 300 GHz. The Industrial, Scientific and Medical (ISM) frequency bands are designated radio bands set aside for non-telecommunication purposes defined by the ITU Radio Regulations. The most common ISM bands are known to be 900MHz and 2.56 GHz. Although the higher frequency waves allow faster vibration of water molecules and thus higher rate of temperature increase in the soil sample, they result in higher attenuation of the signal. As an example, Falciglia (2016) used 2.56GHz MW and observed negligible thermal effects past a maximum distance of 0.2m

As this research aimed to limit the maximum temperature of the clay to 176 ^{o}F, an excessive heating rate was not required and hence a 900 MHz frequency was selected. This allowed for an adequate heating rate while maintaining a low attenuation.

3.3 Experiment Layout

The physical layout of the model experiment is shown in Fig 3.3, A Motorola Quantar T5365A 900MHz 100W Repeater was modified to generate and amplify a 900 MHz signal. This signal was then sent to the transmitting antenna which irradiated the clay sample. Thermistors were inserted into the soil sample to measure its temperature distribution with time. The MW transmission was turned when the maximum soil temperature reached 80 ^{o}C and turned back on at 75 ^{o}C. This allowed for the clay sample to be kept at an elevated temperature range while ensuring that the pore water did not reach a boiling point, which would have resulted in a rapid rise and subsequent explosive release of built up pore pressure. Weights were placed on top the sample to increase the effective stress on the clay.

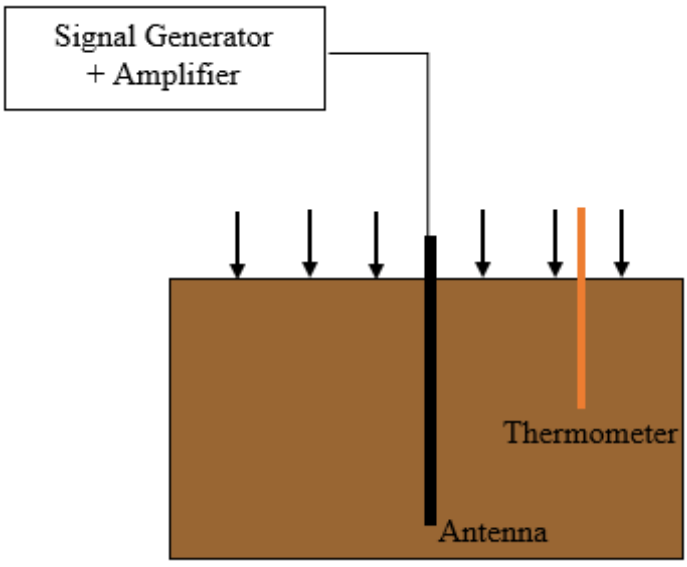

Figure 3.3 Schematic layout of experimental setup

3.3.1 Fabrication of the Faraday Cage

The transmitted power permitted in ISM bands is regulated by Part 15 of the Federal communications commission (FCC) rules which limit ISM band 902-928MHz emissions to 1 Watt. Therefore, to be compliant, the clay sample was enclosed in a well-grounded, copper mesh (mesh spacing=0.2in, maximum allowable mesh spacing = 0.6 inch for 900MHz MW) faraday cage. The faraday cage was grounded using gage 4 copper rods welded to the mesh.

(a) (b)

Figure 3.4 (a) Faraday cage and (b) grounding rod

3.4 Experimental Procedure

3.4.1 Control Experiment (Test 1)

Initially, a 5-gal plastic bucket of diameter 10.8 inches, lined with a drainage cloth, was filled with 80-20 Kaolin-Sand mixture of 16 kN/m^3 up to 9.4 inches in height. A polythene membrane was placed flushed with the top surface of the clay to impose a no-flow boundary condition. The antenna was inserted at the center of the clay sample with care taken to not flush the clay with the antenna surface thus creating a free draining boundary at the antenna. A circular wooden disk was then placed on top of the soil for even application and transfer of loads to the soil.

(a) (b)

Figure 3.5 Plastic bucket (a) lined with drainage cloth and (b) filled with 9.4inch of saturated clay

(a) (b)

Figure 3.6 (a) Sample preparation with polythene barrier with (b) wooden disk and antenna inserted in place

Five digital thermometers were inserted at a depth of 4 inches at varying radial distances of 20, 40, 65, 90 and 110mm as shown in Fig 3.7 from the center of the sample and the disk was loaded with 6 kg of weights. The entire sample was then insulated using fiberglass. The sample was then heated by MW irradiation via the antenna and the temperature readings were recorded at 10 min time intervals.

(a) (b)

Figure 3.7 (a) Thermometers inserted into the clay and (b) radial arrangement of thermometers

3.4.2 Comparison Experiment

For comparison of both the magnitude and rate settlement of the clay under identical loading conditions with and without MW heating a comparison experiment was conducted. Fig. 3. shows the two experiments. It must be noted that the only set of weights have been moved onto the heated sample when the picture was taken.

(a) (b)

Figure 3.8 (a) Non-heated sample and (b) MW irradiated (heated) sample enclosed in a faraday cage

3.4.2.1 Irradiated Sample (Test 2.1)

First the antenna was inserted to the center of the soil sample. The height of the soil sample was identical to the effective length of the antenna. Next a circular wooden disk was placed on top of the soil for even application and transfer of loads. A digital thermometer was inserted 20mm radially outwards from the circumference of the antenna to monitor the temperature. The top and

circumferential surface of the sample was then insulated using fiberglass. Weights were placed on 3 pillars symmetrically erected on the wooden disk. A tube was inserted to facilitate the addition of water to the inner gap of the sample to ensure saturation of the sample for the duration of the experiment. Finally, the setup was completed by assembling the faraday cage around the sample.

(a) (b)

Figure 3.9 a) Sample preparation with polythene barrier and (b) wooden disk, antenna and thermometer in place

(a) (b)

Figure 3.10 (a) Insulated sample and (b) sample with the tube inserted.

Figure 3.11 Loaded sample enclosed in the faradey cage

The repeater was turned on and the sample was irradiated immediately following the cage assembly. The repeater was kept on until the thermometer reading reached 80 °C and then toggled between ON and OFF positions to maintain the temperature between 80-76 °C. A laser distance measuring device was placed on a mounted glass plate. Vertical distance measurements were taken at 3 marked points along the periphery of the circular weights (Fig. 3.13b) to monitor the settlement of the samples (further elaborated in section 3.5) Data was taken at 15 min time intervals for the first 3 hrs and then the data acquisition time interval was increased to 5 hrs and 8 hrs after 24 hrs and 48 hrs respectively.

3.4.2.2 Non-irradiated Sample (Test 2.2)

A PVC pipe with diameter identical to the antenna was inserted at the center of the soil sample (Fig. 3.12a) to maintain identicality with the irradiated sample. The wooden disks and weights were placed on the sample similarly to Test 2.1 (Fig. 3.12b). Vertical distance measurements were taken identically to the previous test at 3 marked locations around the periphery of the circular disks at similar time intervals.

(a) (b)

Figure 3.12 (a) Sample with inserted PVC pipe and (b) loaded sample

3.5 Measurement of Rate of Consolidation

Consolidation of the clay samples is reflected by the pore pressure dissipation and the overall height reduction of the sample. For the pore pressure range of this experiment (<3psi) piezometers are large in dimension and inserting them into the soil sample could disrupt the fluid flow and may also lead to uneven settling. Additionally, the incident high power electric field may

affect the piezo-metric readings. Therefore, traditional pore pressure transducers were not used in this experiment. This could have been overcome by inserting a capillary tube into the soil sample which extends out of the faraday cage and connects to a piezometer. However, there could have been practical difficulties related to this approach leading to erroneous readings for such low pore pressure values as the setup must be completely sealed ensuring no water is allowed to leak out.

Considering the above factors, the rate of consolidation was measured using the height of the clay sample. Commonly used LVDT sensors cannot be used in this experiment as they are known to be sensitive to external magnetic fields. Thus a laser distance sensor of resolution 0.0001mm was used. Utilizing a laser sensor allowed the unit to be kept outside the faraday cage limiting the influence of the EMWs on the laser sensor.

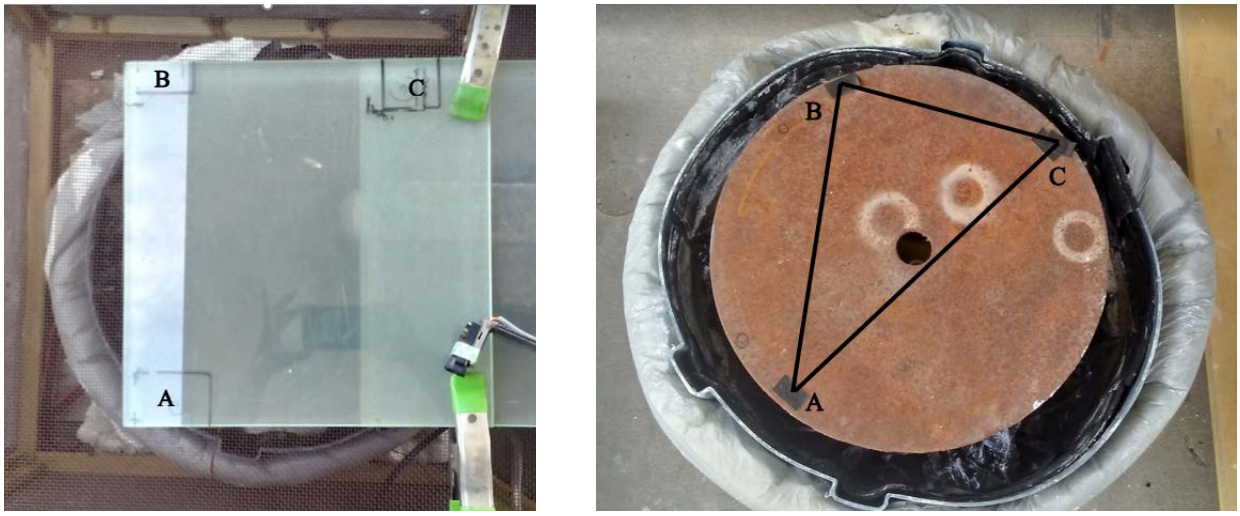

(a) (b)

Figure 3.13 (a) Laser distance sensor mounted glass plate (b) corresponding target points on the sample

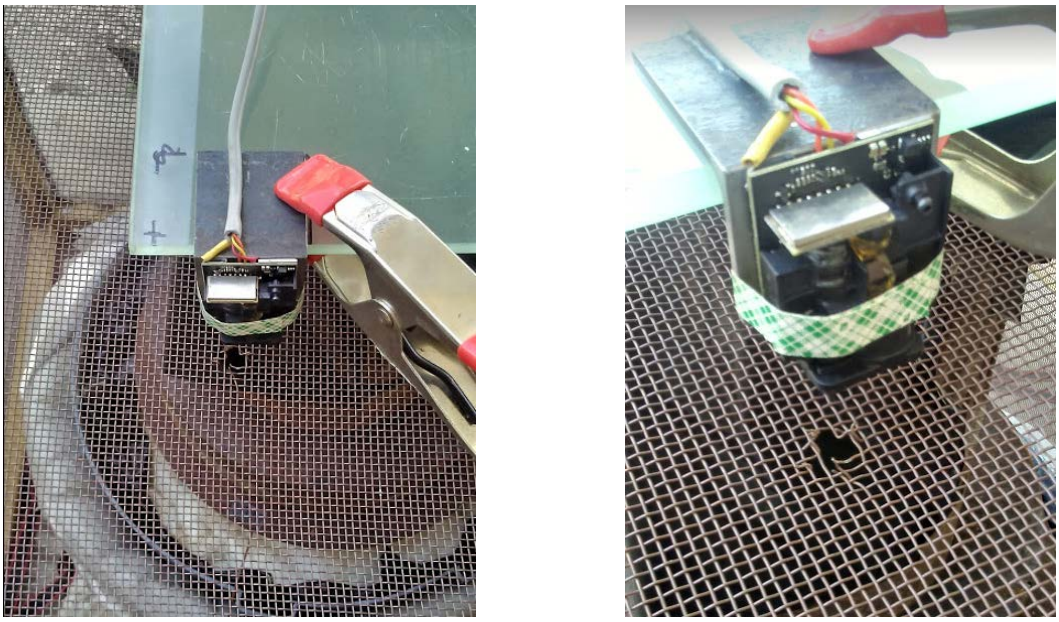

(a) (b)

Figure 3.14 (a) Laser sensor positioned for measurement and (b) close-up view of positioned sensor

CHAPTER 4: RESULTS AND DISCUSSION

4.1 Experimental Results of Test 1

As discussed in Chapter 3, the variation of temperature of nodes R1-R5 (Fig. 3.7) were measured using 5 thermometers inserted at a depth of 4inches in the test sample. The resultant temperature variations of each node are shown in Fig. 4.1 .

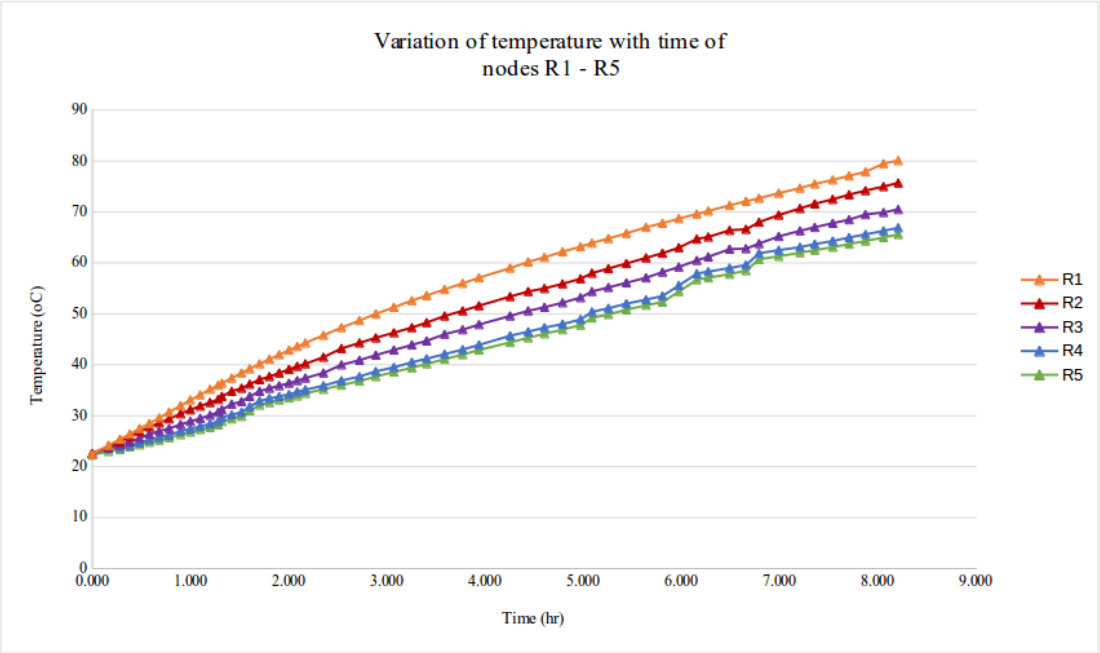

Figure 4.1 Variation of temperature of nodes R1-R5 with time

It can be observed from the results in Fig 4.1 that the temperature at the inner most node (R1) achieved the maximum allowable temperature of 80 ^{o}C in 8.2 hrs while a maximum temperature of 65.6 ^{o}C was achieved at the outermost node (R5).

4.2 Verification of the Numerical Model and the Computer Program

The output of the computer code was compared with the empirical data of Test 1 in order to validate the program results and radial variations of temperature at varying time steps were considered. Data fitting was carried out to determine the unknown coefficients in Eq (10).

4.2.1 Determination of Unknown Coefficients

The values of E_0, ε' and ε'', which governs the variation of temperature, and subsequently, the pore pressure and porosity, were unknown for the clay setup and hence they were determined by fitting experimental and theoretical data. For the node R1, the effects of hydraulic conductivity and coefficient of consolidation would have negligible effects on the temperature variation. Therefore, utilizing the measured values of ε' and ε'' at 25 ^{o}C allowed the accurate determination of the value of E_0 to be 603 V/m. The variations of ε' and ε'', greatly affected by the temperature and frequency of the incident EMWs, were determined by fitting the experimental and numerically predicted temperature variation of the node R1 over the duration of Test 1. The real part of the dielectric permittivity (ε') was kept constant [3] and the imaginary part (ε'') was varied to fit the data. This variation, shown in Fig 4.2 was then included in the computer program to predict nodal temperatures of the rest of the nodes.

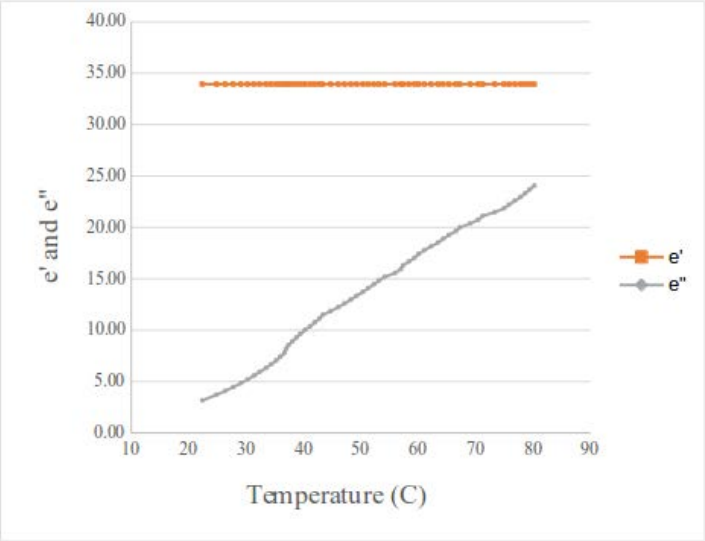

Figure 4.2 Variation of ε' and ε'' with temperature for E_0=603 V/m

The radial variations of temperature at varying time steps were then considered to validate the numerical model. These are shown in Fig 4.3.

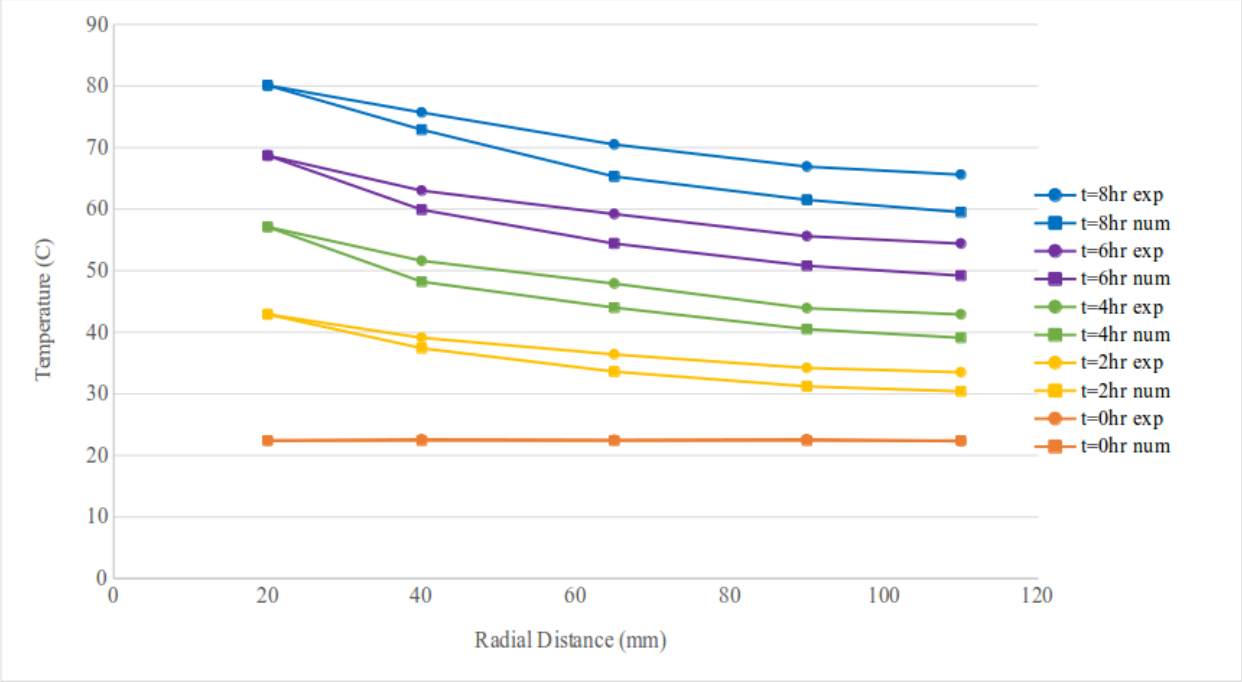

Figure 4.3 Numerical temperature variations vs. experimental data

It can be observed from Fig 4.3 that the numerical model prediction and empirical data are in good agreement initially. For longer times it can be observed that the results deviate increasingly. However, it can be seen that the exponential decreasing trend of the temperature holds in each case. The above deviation maybe due to practical errors in the experiment. The numerical model assumes a uniform sample, however, as the clay sample was packed manually, inconsistencies in density and porosity of the sample could have resulted. Above reasons may have caused deviations in the temperature increase in addition to causing disruptions to microwave propagation.

4.3 Computational Results

The analytical model was used to predict the temperature, pore pressure and porosity of the clay sample. Fig.4.4 shows the variation of pore pressure and temperature of the node at r=21 with time for a duration of 8 hrs predicted by the model. It can be seen that the temperature increases steadily with time whist the pore pressure reaches a peak value. Initially, the pore pressure of the sample rises as the temperature increased due to differential thermal expansion of clay. However, the temperature rise also results in the increase of the hydraulic conductivity of soil and with time the effects of the hydraulic conductivity takes prominence and the pore water dissipation causes a decrease in pore pressure. The radial variations of temperature, pore pressure and porosity at 4 hr, 6 hr and 8 hr time intervals as predicted by the model are depicted in Fig 4.5.

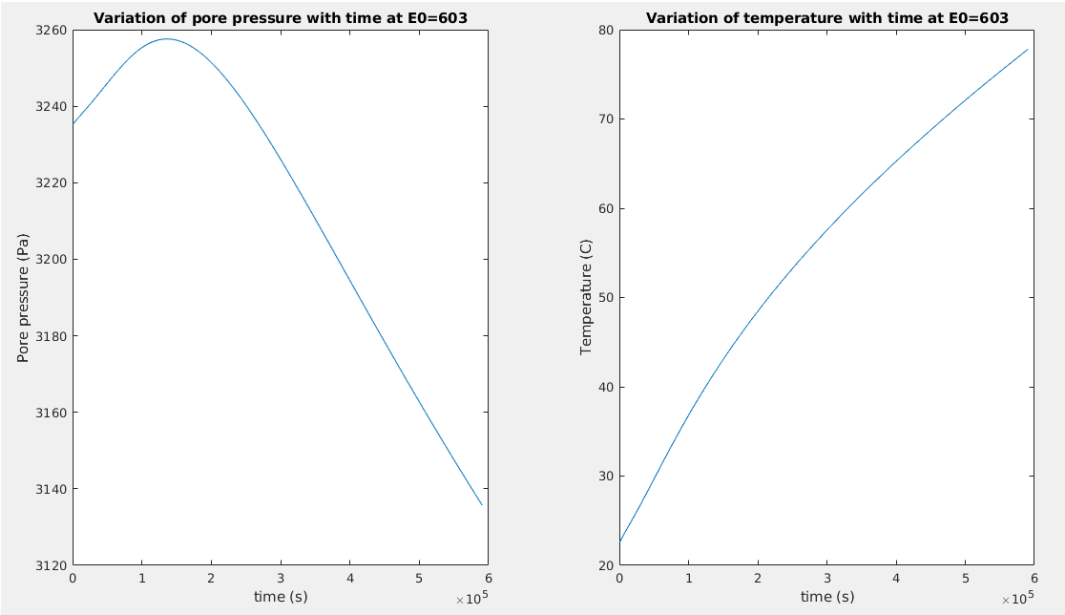

(a) (b)

Figure 4.4 The variation of (a) pore pressure and (b) temperature of node 21 with time

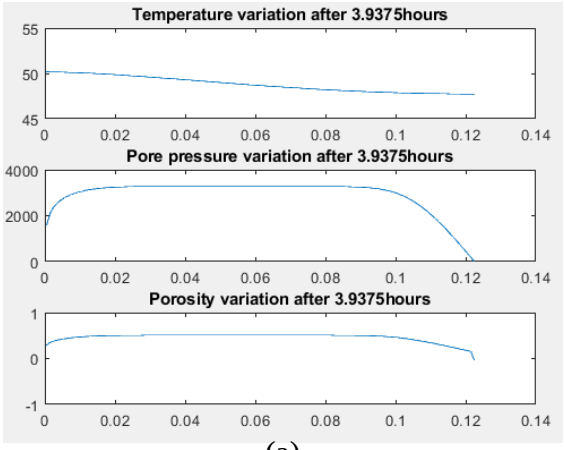

(a)

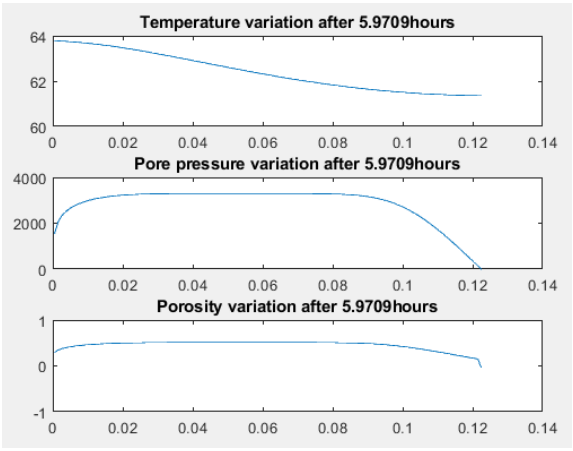

(b)

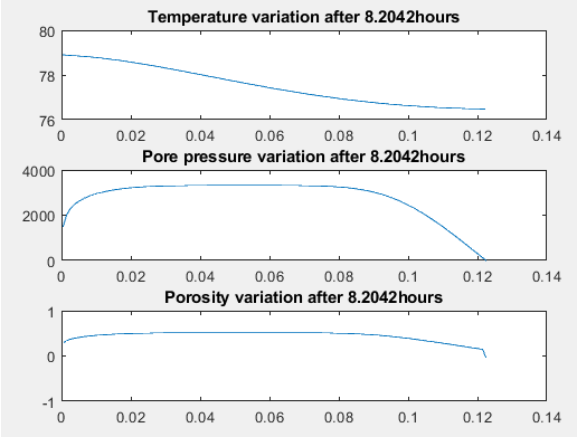

(c)

Figure 4.5 Analytical model predictions of the variation of tempertaure, pore pressure and porosity for times (a) 4 hr, (b) 6 hr and (c) 8 hr

4.4 Parametric Study

A parametric study was conducted to investigate the influence of the significant parameters on the variation of temperature and pore pressure in the clay sample. The variation of temperature is highly dependent on the incident electric field strength(E_0). A higher E_0 value would result in elevated temperatures for a given duration of irradiation. This phenomenon is accurately represented by fig 4.6 which shows the radial variation of temperature predicted by the analytical model at a selected time of 5.5hrs.

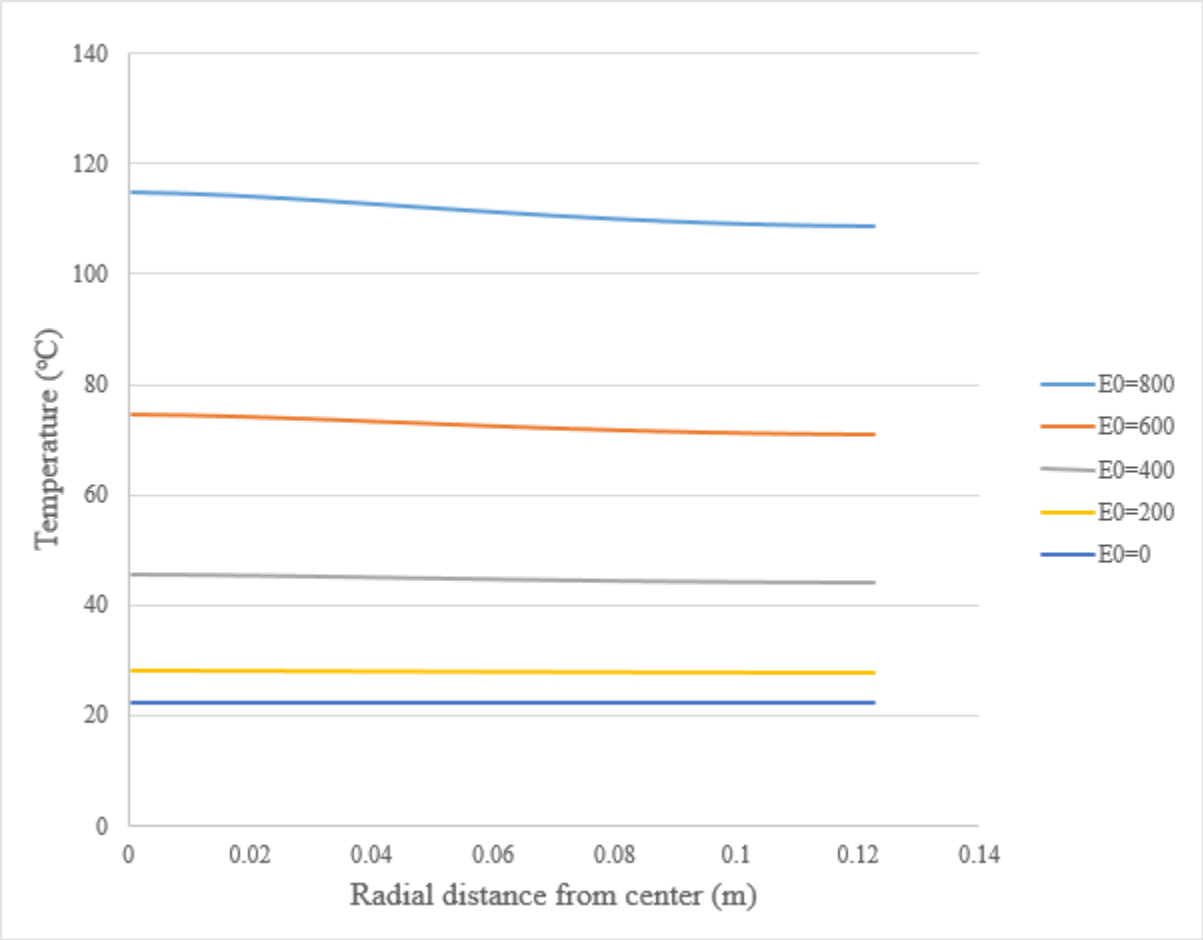

Figure 4.6 Radial variation of temperature for varying electric field strengths at time = 5.5hrs.

The pore pressure distribution within the clay is greatly influenced by the hydraulic conductivity of the clay. An increased hydraulic conductivity of the sample will result in an increase of the rate of pore pressure dissipation. This is accurately represented by fig 4.7 which depicts the radial variation of pore pressure predicted by the analytical model for varying hydraulic conductivities at time = 8 hrs.

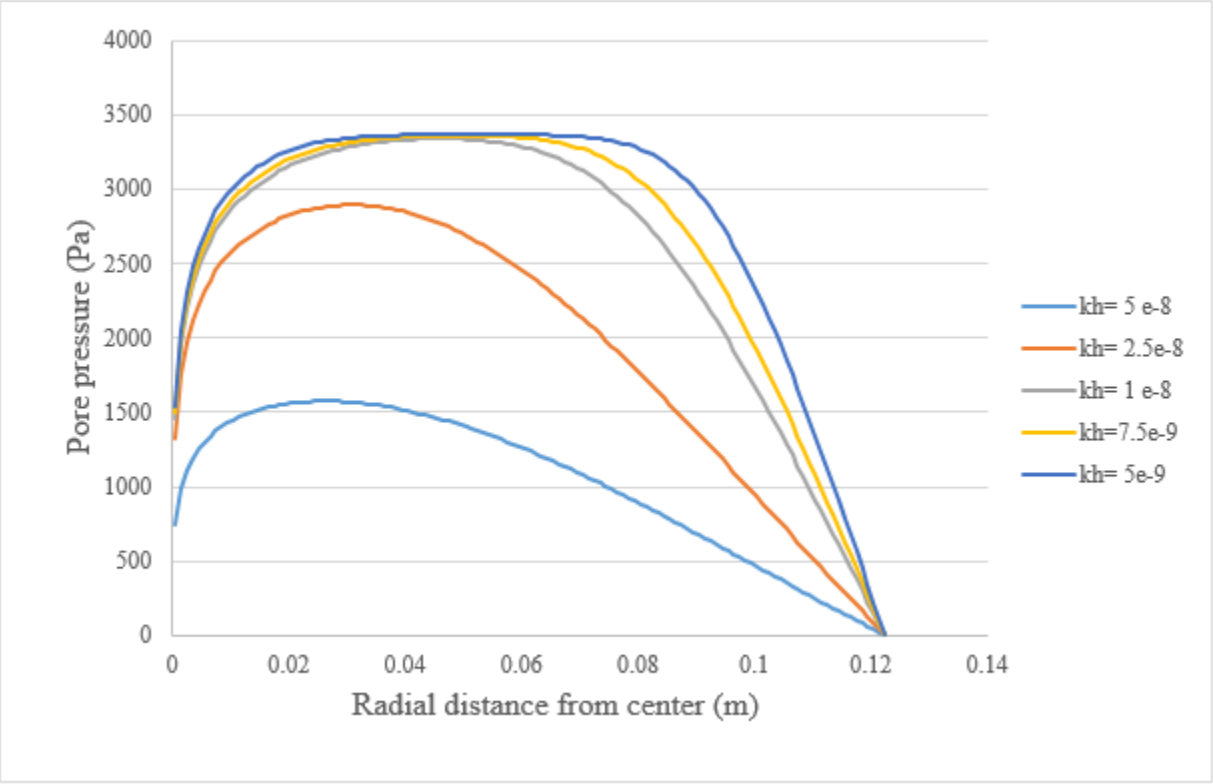

Figure 4.7 Radial variation of pore pressure with time for different hydraulic conductivity values

4.5 Experimental Results of Heated/Non-heated Samples (Test 2.1 and Test 2.2)

The experimental data and the analysis to predict the settlement of the soil samples are presented in the following section.

4.5.1 Variation of Vertical Height Measurements

As discussed in Chapter 3, the rate of consolidation of the samples were monitored using a laser distance sensor at 3 representative locations on the surface of the sample. The measured vertical height variation of the 3 locations of the non-heated and heated samples are summarized in Fig. 4.8 and Fig. 4.9 respectively.

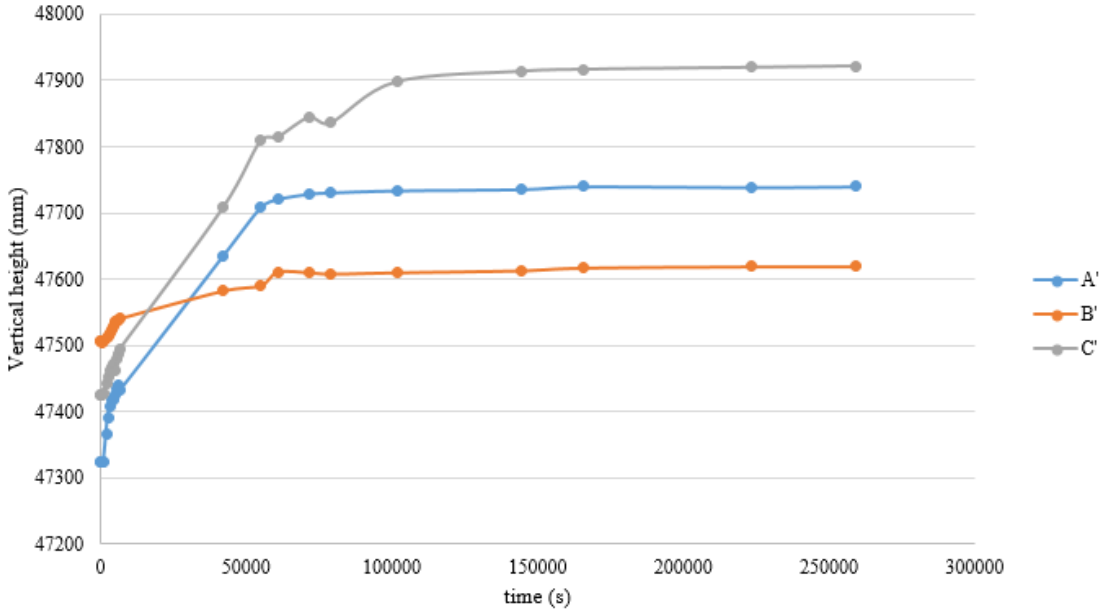

Figure 4.8 Vertical height variation of 3 marked locations of non-heated sample

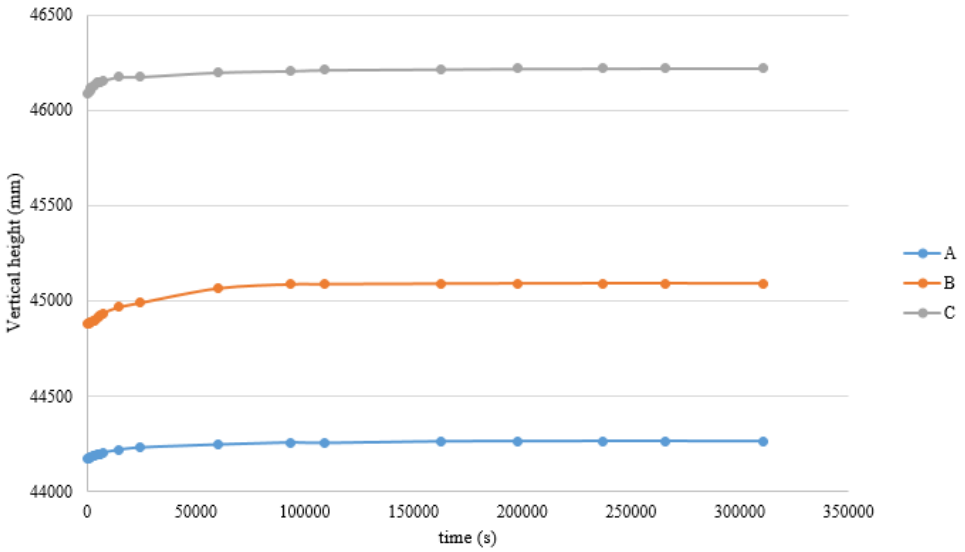

Figure 4.9 Vertical height variation of 3 marked locations of heated sample

The consolidation of the clay sample would result in vertical height change of the surveyed locations. This is reflected in Fig 4.8 and Fig 4.9. The overall settlements of the clay samples were evaluated by considering the percentage variation of a representative volume of the clay sample. The percentage variation of a representative volume with time is plotted in Fig 4.10 .

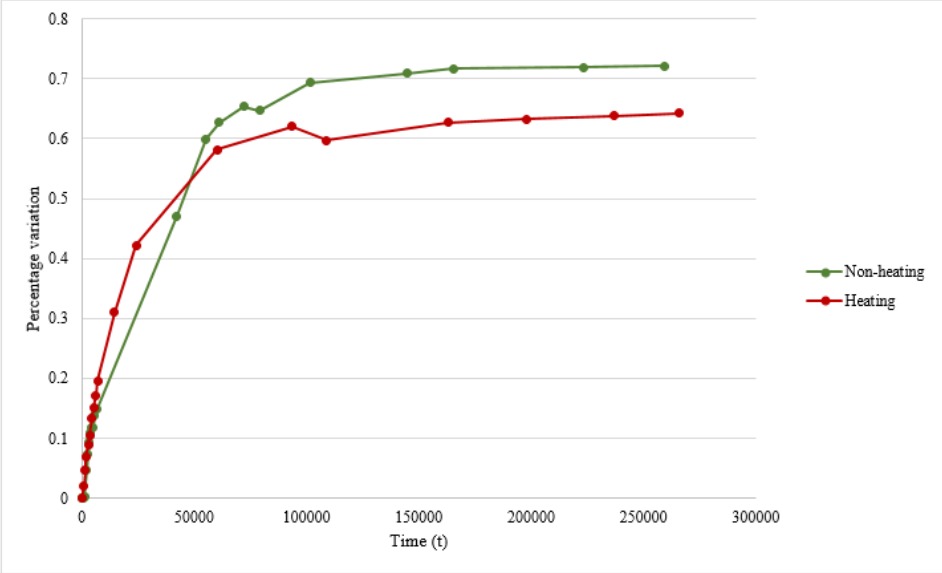

Figure 4.10 Percentage variation of a representative volume with time

Per Federal Communications Commission requirements, the sample with MW irradiation (heating) was to be carried out while the sample was enclosed in a faraday cage, therefore, the cage was assembled around the sample prior to heating of the sample. It is noted that due to measurements being recorded after the faraday cage was assembled, a time of 35min elapsed from the time the samples were loaded to the first measurement. Therefore, a correction of height measurements to include the settlement during the initial 35 min was needed. This was achieved by back extrapolating the measured data trends up to time zero. The resultant decrease in percentage of consolidation of a representative volume is shown in Fig 4.11.

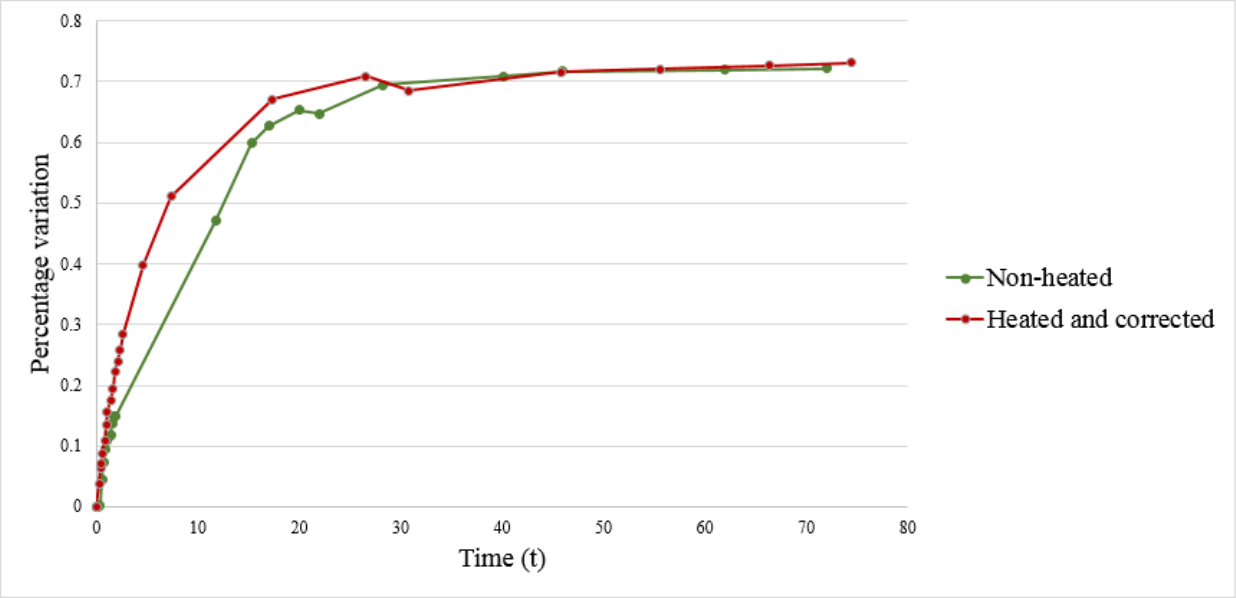

Figure 4.11 Modified percentage variation in volume of the two samples plotted against time

The ultimate consolidation of a clay sample can be calculated using Eq. (19),

$$S_c = \frac{C_c H}{1 + e_0} \log\left(\frac{\sigma_0' + \Delta\sigma'}{\sigma_0'}\right) \tag{19}$$

where, $C_c$is the compression index, H is the saturated clay layer thickness, e_0 is the initial void ratio, σ_0' is the initial effective overburden pressure and $\Delta\sigma'$ is the increase in effective pressure due to the added load.

It is evident from Eq. (19) that the ultimate consolidation is dependent only upon soil parameters and therefore, the ultimate percentage settlement of both the heated and non-heated samples could be expected to be equal. Additionally, the introduction of heating is expected to generate excess pore pressure and increase the hydraulic conductivity resulting in an increase of the rate of dissipation of excess pore pressure. These expectations are seen to be accurately represented by the results in Fig 4.11 which depicts that the percentage variations of the two samples ultimately reach the same value while the rate of settlement is higher for the heated sample. However, it must be noted that as the consolidation process is irreversible, only a single experiment was conducted for this work and as such, a confidence interval cannot be drawn.

The rate of settlement could also be represented by the change in the area under the pore pressure diagram predicted by the analytical model. The percentage change of the area under the analytically predicted pore pressure curve representing the dissipated pore pressure is presented in Fig. 4.12. (Calculations of which are presented in Appendix B). The introduction of heating is expected to dissipate pore pressure at a higher rate. Therefore, the rate of percentage change of the representative area under the pore pressure curve is expected to be higher. These expectations are accurately represented by Fig. 4.12.

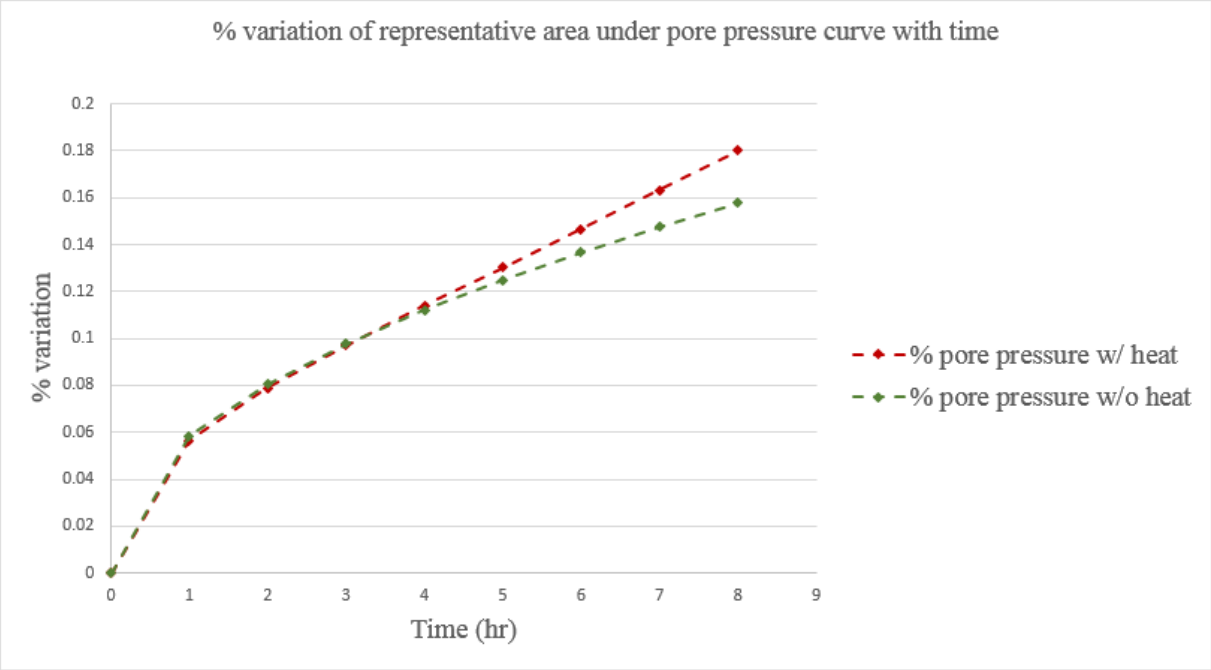

Figure 4.12 Variation of the percentage change of an area representative of the dissipated pore pressure with and without heating as predicted analytically

CHAPTER 5: CONCLUSION

This research aimed to study the feasibility of utilizing microwaves to expedite the excess pore pressure dissipation and hence the consolidation of clay. A numerical model has been formulated and implemented using finite differencing methods to theoretically predict the temperature rise and pore pressure dissipation due to MW heating.

The feasibility of utilizing microwaves to raise the temperature of a clay sample was also evaluated practically by conducting bench-scale experiments. The use of microwave irradiation to rapidly increase the temperature of saturated clay was quantified in this research with temperatures of 80 ^{o}C being achieved after 8 hrs of soil irradiation. This proved to be more efficient than current soil heating methodologies. The effects of MW on the settlement of the clay was evaluated by conducting two comparable consolidation experiments. Considering the percentage variation of a representative volume of each clay sample, it was observed that increasing the temperature of the clay sample using MW heating resulted in a higher rate of settlement when compared with the settlement of the non-heated sample while the ultimate percentage settlement of both were more or less the same. Considering the area under the pore pressure variation curve representative of the dissipated pore pressure, the analytical predictions showed a higher rate of pore water dissipation for a heated clay sample. The predictions of the numerical model are in good correlation with the corresponding experimental data.

REFERENCES

[1] Falciglia PP, Scandura P, Vagliasindi FGA. Modelling of in situ microwave heating of hydrocarbon-polluted soils: Influence of soil properties and operating conditions on electric field variation and temperature profiles. J Geochemical Explor 2017;174:91–9. doi:10.1016/j.gexplo.2016.06.005.

[2] Barba AA, Acierno D, D'Amore M. Use of microwaves for in-situ removal of pollutant compounds from solid matrices. J Hazard Mater 2012;207–208:128–35. doi:10.1016/j.jhazmat.2011.07.123.

[3] Seyfried MS, Grant LE. Temperature Effects on Soil Dielectric Properties Measured at 50 MHz. Vadose Zo J 2007;6:759. doi:10.2136/vzj2006.0188.

[4] Abuel-Naga, H. M., Bergado, D. T., & Chaiprakaikeow, S. (2006). Innovative Thermal Technique for Enhancing the Performance of Prefabricated Vertical Drain during the Preloading Process. Geotextiles and Geomembranes, 359-370.

[5] Abuel-Naga, H. M., Bergado, D. T., Bouazza, A., & Ramana, G. V. (2007). Volume Change Behaviour of Saturated Clays Under Drained Heating Conditions: Experimental Results and Constitutive Modeling. Canadian Geotechnical Journal, 942-956

[6] Metaxas, A.C., Meredith, R.J., 1993. Industrial Microwave Heating. IEE Power Engineering Series Vol. 4. Peter Pregren LTD, London..

[7] J.P. Robinson, S.W. Kingman, E.H. Lester, C. Yi. Microwave remediation of hydrocarbon contaminated soils – scale up using batch reactors. Sep. Purif. Technol., 96 (2012), pp. 12-19, 10.1016/j.seppur.2012.05.020

APPENDIX A: MATLAB CODE

The Matlab code used to analyse the numerical model is given below.

```
%% INPUTS ----------------------------------------------------------------
tic
% Sure inputs:
z=0.11938;              % Height of soil above (m), taken as half the clay size of the test sample.@@
cw=4184;                % Specific heat cap of water J/kg/K@@
rhos=2650;              % Density of dry Kaolin kg/m3 @@
T0=22.5;                % Initial temperature (Celsius)@@
Ta=22.5;                % Ambient temperature (Celsius)@@
Tp=22.5;                % Initial temperature of plastic@@
W=10;                   % Weight placed on sample(kg)
w=5654866776.46;    % Annular frequency (rad/s) = 2*pi*f @@
e0=8.8541878176e-12;% Dielectric permitivity of free space (F/m)@@
ep=33.93;               % Real part of the relative dielectric permitivity.
epp=3.72;               % Imaginary part of the relative dielectric permitivity.
lamda=0.333;            % Wavelength of the MW. (m)@@
La=0.014;               % Radius of antenna (m)
L=0.137-La;             % Max radial length of sample (m)= (radial length of clay measured - radius of
antenna)
k=1.2;                  % Thermal conductivity (W/mK) of Kaolin clay with 80% sand:
https://www.tandfonline.com/doi/pdf/10.1080/1064119X.2015.1033072?needAccess=true@@
% kh @ 25 =7.8e-9;    %3.26e-9; % Hydraulic conductivity of kaolin
(m/s)  http://www.ejge.com/2012/Ppr12.068alr.pdf.
                        % K70S20 = 3.6e-10, K100S0 = 2.6e-10. Linearly interpolated.
gc=16000;               % Specific weight of clay. (N/m3)

gw=9810;                % Specific weight of water. (N/m3)@@ Is a function of T.
https://www.engineeringtoolbox.com/water-density-specific-weight-d_595.html,
                        % Drawn on excel for empherical formula: gw = -0.000001257094674467 22*T^4
+ 0.000403040504841412*T^3 - 0.0734914863970049*T^2 + 0.502255621126391*T +
9,805.36629538316
alphaw=5.16/10000;      % Coefficient of thermal expansion of water.(/K) Is a function of T.
https://www.engineeringtoolbox.com/water-density-specific-weight-d_595.html,
                    % Drawn on excel for empherical formula: alphaw = (-0.000000068260086*T^4 +
0.000018582195265*T^3 - 0.002135775005238*T^2 + 0.173020160507236*T -
0.672871058607526)/10000
```

```
rhop=950;                % density of plastic, kg/m3,@@  http://www.goodfellow.com/E/Polyethylene-High-density.html
cp=1900;                 % cp of plastic, J/kg/K,@@  http://www.goodfellow.com/E/Polyethylene-High-density.html
rhow=985;                % Density of water kg/m3.@@ Density change from 996 to 968 for 27C - 8%C. Average taken.
n0=0.5;                  % Initial porosity of the sample@@
cs=1010;                 % Specific heat cap of Kaolin@@ (J/kg/K) at room temp. https://vdocuments.site/thermal-conductivity-and-specific-heat-of-kaolinite-evolution-with-thermal.html
E0=603;                  % V/m
c=0.5;                   % Constant

%% GRID FORMING INPUTS ----------------------------------------------------------------

% l is the physical length from the actual beginning point of the sample.
% all l are the length to the element size changing point in r direction.
% Make sure these can be divided by d to get integers.
l1=0.1;
l2=2*l1;
l3=L;
% all d are the element sizes in the r direction
d1=0.001;
d2=d1;
d3=d1;
% all v are the lenth to the element size changing point in t direction
v3=29880;
v1=v3/4;
v2=v3/2;

% all h are the element sizes in the t direction
h1=0.1;
h2=h1;
h3=h1;


%% Forming arrays and preliminary grids ---------------------------------

P1  = W*9.81/(pi*L^2); % Pressure after weight placement = Weight*g/area_applied
% sig = 4;                    % Effective stress at z meters below the sample surface
P1+gw*z;
sig=P1+gc*z;
%u=P1+gw*z; % t goes from 0-m3
m1=v1/h1;
m2=m1+((v2-v1)/h2);
m3=m2+((v3-v2)/h3);
% r goes from 1-n3
n1=(l1/d1);
n2=n1+((l2-l1)/d2);
n3=n2+((l3-l2)/d3);
```

```
T=zeros(n3+1,m3+1);
T(1:n3,1)=T0;
T(n3+1,1)=Tp; %n3+1 node is the plastic. Which at t=1 is at Tp
u=zeros(n3+1,m3+1);
u(1:n3,1)= P1+gw*z;
u(n3+1,1:m3+1)=0;
n=zeros(n3+1,m3+1);
n(1:n3,1)=n0;


% Then make a set of arrays:
% R (distance to the node from the beginning)
% p (the length of the grid infront of the node point)
% Then these can be called to solve the unequal grid point for any node
% Remember when calling a node it has to be p(r) is the forward grid size,
% p(r-1) is the behind grid size

p=zeros(1,n3);
for i=1:n1-1
   p(int16(i))=d1;
end

for i=n1+1:n2-1
   p(int16(i))=d2;
end

for i=n2+1:n3-1
   p(int16(i))=d3;
end
p(n1)=(d1+d2)/2;
p(int16(n2))=(d2+d3)/2;
p(int16(n3))=d3;


R=zeros(1,n3);
for i=1:n1
   R(int16(i))=(2*i-1)*d1/2;
end

for i=n1+1:n2
   R(int16(i))=n1*d1+((2*(i-n1)-1)*d2/2);
end

for i=n2+1:n3
   R(int16(i))=n1*d1+((n2-n1)*d2)+((2*(i-n2)-1)*d3/2);
end
```

```
aaaTherm1=0.02/d1+1; %Therm1 at R= 20mm, then r=20mm/d1
ttt=m3; %time considered in code
hours=ttt*h1/3600
seconds=ttt*h1;
aaa=1;

%%   t=1:m3 Code with simultaneously solved T , u and n ----------

r2=zeros(ttt+1,1);
r4=zeros(ttt+1,1);
r6=zeros(ttt+1,1);

t2=zeros(ttt+1,1);
t4=zeros(ttt+1,1);
t6=zeros(ttt+1,1);

k2=zeros(ttt+1,1);
k4=zeros(ttt+1,1);
k6=zeros(ttt+1,1);


% for t=1:m3 the forward differencing parts are all h1 in length
for t=1
   dp=lamda*sqrt(ep)/(2*pi*epp);
   for r=1:n3
      epp=-0.000607526051132*T0^2 + 0.235065134973541*T0 - 3.9933369776088150;
      a=n(r,t)*rhow*cw+rhos*cs;
      v=k*h1*(1/d3^2+1/(2*R(r)*d3));
      m=-d3^2*rhop*cp/(k*h1);

%        temperature eqn
      if r==1
         T(r,t+1)= (((k*h1/d1^2+k*h1/(2*R(r)*d1))*T(2,t))+((a-k*h1/d1^2-
k*h1/(2*R(r)*d1))*T(1,t))+(w*e0*epp*(E0^2)*h1*exp(-2*R(r)/dp)))/a;%checked

      elseif r==n3
         T(r,t+1)= (((a-2*k*h1/d3^2)*T(r,t))+((k*h1/d3^2-k*h1/(2*R(r)*d3))*T(r-
1,t))+(v*Tp)+(w*e0*epp*(E0^2)*h1*exp(-2*R(r)/dp)))/a; %checked
         T(r+1,t+1)= Tp+(1/m)*T(r,t)-(1/m*T(r-1,t)); %checked

      else
         p1=k/(p(r-1)*p(r)*(p(r-1)+p(r)));
         T(r,t+1)= (((2*p1*p(r-1)+p1*(p(r-1))^2/R(r))*T(r+1,t))+((p1*((p(r))^2-(p(r-1))^2)/R(r)-
2*p1*(p(r-1)+p(r))+a)*T(r,t))+((2*p1*p(r)-p1*(p(r))^2/R(r))*T(r-1,t))+(w*e0*epp*(E0^2)*exp(-
2*R(r)/dp)*h1))/a; %checked
      end

% %       This bottom part allows to track the change of temperature of a specific node. Or three nodes for
now.
```

```
    if r==aaaTherm1
       t2(t,1)=T(r,t);
    elseif r==aaa-1
       t4(t,1)=T(r,t);
    elseif r==aaa-2
       t6(t,1)=T(r,t);
    end


%       flow eqn
    gw = -0.00000125709467446722*(T(r,t))^4 + 0.00040304050484841412*(T(r,t))^3 -
0.0734914863970049*(T(r,t))^2 + 0.502255621126391*(T(r,t)) + 9805.36629538316;
    kh=0.000000000001244153813550590000*(T(r,t))^2 +
0.000000000075945707518922500000*T(r,t) + 0.000000005187823391736720000000;
    f=kh*R(r)/(gw*d1^2);
    sigminu = (sig-u(r,t));


    b=c*R(r)*((1-n(r,t))^2)/(h1*(sigminu));
%     alphaw=((-0.000000068260086*(T(r,t))^4 + 0.000018582195265*(T(r,t))^3 -
0.002135775005238*(T(r,t))^2 + 0.173020160507236*(T(r,t)) - 0.672871058607526)/10000)/2;

    if r==1
       u(1,t+1)= (((b-2*f)*u(1,t))+((f+kh/(2*gw*d1))*u(2,t))-(n(r,t)*alphaw*R(r)/h1*(T(1,t+1)-
T(1,t))))/b;%checked

    elseif r>=2 && r<=n3-1
       q=kh/(gw*p(r-1)*p(r)*(p(r-1)+p(r)));
       u(r,t+1)= (((b-2*R(r)*q*(p(r-1)+p(r))+q*((p(r))^2-(p(r-1))^2))*u(r,t))+((2*R(r)*q*p(r-1)+q*(p(r-
1))^2)*u(r+1,t))+((2*R(r)*q*p(r)-q*(p(r))^2)*u(r-1,t))-(n(r,t)*alphaw*R(r)/h1*(T(r,t+1)-T(r,t))))/b;
%checked

    end

%       This bottom part allows to track the change of pore pressure of a specific node. Or three nodes for
now.

    if r==aaaTherm1
       r2(t,1)=u(r,t);
    elseif r==aaa-1
       r4(t,1)=u(r,t);
    elseif r==aaa-2
       r6(t,1)=u(r,t);
    end

%       porosity eqn
    n(r,t+1)=(u(r,t+1)-u(r,t))/((sigminu)/(c*((1-n(r,t))^2)))+n(r,t);

    if r==1
```

```
%            disp(n(1,t+1))
          k2(t,1)=n(r,t);
%
       end

    end

end

% The below ttt part allow  the code to run only till that time step.
% Putting ttt= m3 runs it till the predefind end of time.
% The plot ss part plots the last column.

for t=2:ttt
    dp=lamda*sqrt(ep)/(2*pi*epp);   % Depth of penetration

    for r=1:n3
       epp=-0.000607526051132*T(r,t-1)^2 + 0.235065134973541*T(r,t-1) - 3.9933369776088150;
       a=n(r,t)*rhow*cw+rhos*cs;
       v=k*h1*(1/d3^2+1/(2*R(r)*d3));
       m=-d3^2*rhop*cp/(k*h1);

%         temperature eqn
       if r==1
          T(r,t+1)= (((k*h1/d1^2+k*h1/(2*R(r)*d1))*T(2,t))+((a-k*h1/d1^2-
k*h1/(2*R(r)*d1))*T(1,t))+(w*e0*epp*(E0^2)*h1*exp(-2*R(r)/dp)))/a; %checked
       elseif r==n3
          T(r,t+1)= (((a-2*k*h1/d3^2)*T(r,t))+((k*h1/d3^2-k*h1/(2*R(r)*d3))*T(r-
1,t))+(v*T(r+1,t))+(w*e0*epp*(E0^2)*h1*exp(-2*R(r)/dp)))/a; %checked
          T(r+1,t+1)= T(r+1,t)+(1/m*T(r,t))-(1/m*T(r-1,t)); %checked

       else
          p1=k/(p(r-1)*p(r)*(p(r-1)+p(r)));
          T(r,t+1)= (((2*p1*p(r-1)+p1*(p(r-1))^2/R(r))*T(r+1,t))+((p1*((p(r))^2-(p(r-1))^2)/R(r)-
2*p1*(p(r-1)+p(r))+a)*T(r,t))+((2*p1*p(r)-p1*(p(r))^2/R(r))*T(r-1,t))+(w*e0*epp*(E0^2)*exp(-
2*R(r)/dp)*h1))/a; %checked
       end

% %        This bottom part allows to track the change of temperature of a specific node. Or three nodes for
now.
       if r==aaaTherm1
          t2(t,1)=T(r,t);
       elseif r==aaa-1
          t4(t,1)=T(r,t);
       elseif r==aaa-2
          t6(t,1)=T(r,t);
       end

%         flow eqn
```

```
    gw = -0.00000125709467446722*(T(r,t))^4 + 0.00040340504841412*(T(r,t))^3 -
0.0734914863970049*(T(r,t))^2 + 0.502255621126391*(T(r,t)) + 9805.36629538316;
    kh=0.000000000001244153813550590000*(T(r,t))^2 +
0.000000000075945707518922500000*T(r,t) + 0.000000005187823391736720000000;
    f=2*kh*R(r)/(gw*d1^2);
    sigminu = (sig-u(r,t));

    b=c*R(r)*((1-n(r,t))^2)/(h1*(sigminu));
%       alphaw=((-0.000000068260086*(T(r,t))^4 + 0.000018582195265*(T(r,t))^3 -
0.002135775005238*(T(r,t))^2 + 0.173020160507236*(T(r,t)) - 0.672871058607526)/10000)/2;

    if r==1
       u(1,t+1)= (((b-2*f)*u(1,t))+((f+kh/(2*gw*d1))*u(2,t))+(n(r,t)*alphaw*R(r)/h1*(T(1,t+1)-
T(1,t))))/b;%checked
%
    elseif r>=2 && r<=n3-1
       q=kh/(gw*p(r-1)*p(r)*(p(r-1)+p(r)));
       u(r,t+1)= (((b-2*R(r)*q*(p(r-1)+p(r))+q*((p(r))^2-(p(r-1))^2))*u(r,t))+((2*R(r)*q*p(r-1)+q*(p(r-
1))^2)*u(r+1,t))+((2*R(r)*q*p(r)-q*(p(r))^2)*u(r-1,t))+(n(r,t)*alphaw*R(r)/h1*(T(r,t+1)-T(r,t))))/b;
%checked
    end

%       This bottom part allows to track the change of pore pressure of a specific node. Or three nodes for
now.

    if r==aaaTherm1
       r2(t,1)=u(r,t);
    elseif r==aaa-1
       r4(t,1)=u(r,t);
    elseif r==aaa-2
       r6(t,1)=u(r,t);
    end


%       porosity eqn
    n(r,t+1)=(u(r,t+1)-u(r,t))/((sigminu)/(c*((1-n(r,t))^2)))+n(r,t);
    if r==aaaTherm1
       k2(t,1)=n(r,t);
    end


  end

end

%% Plotting excess pore pressure and writing to excel

% usum=zeros(3,35);
% x=1;
```

```
% for i=1:9001:295351
%     usum(1,x)=(i-1)/36000;
%     usum(2,x)=sum(u(1:n3,i))*d1; % without heating
% %     usum(3,x)=sum(u(1:n3,i))*d1; % heating
%     x=x+1;
% end
% usum=usum'
%

%% Plotting the change of pore pressure/temperature of different nodes with time

figure
ax1 = subplot(1,2,1);
plot(ax1,1:ttt,r2(1:ttt,1))
title(ax1,[ 'Variation of pore pressure with time at E0=' num2str(E0)]);
ylabel(ax1,'Pore pressure (Pa)')
xlabel(ax1,'time (s)')

ax5 = subplot(1,2,2);
plot(ax5,1:ttt,t2(1:ttt,1))
title(ax5,[ 'Variation of temperature with time at E0=' num2str(E0)]);
ylabel(ax5,'Temperature (C)')
xlabel(ax5,'time (s)')

%% Plotting the overall change of pore pressure/temperature of with time


figure
ax1 = subplot(3,1,1);
plot(ax1,R(1,1:n3),T(1:n3,ttt))
title(ax1,['Temperature (C) variation after ' num2str(hours) 'hours'])

ax2 = subplot(3,1,2);
plot(ax2,R(1,1:n3),u(1:n3,ttt))
title(ax2,['Pore pressure (Pa) variation after ' num2str(hours) 'hours'])

ax3 = subplot(3,1,3);
plot(ax3,R(1,1:n3),n(1:n3,ttt))
title(ax3,['Porosity variation after ' num2str(hours) 'hours'])
toc
```

APPENDIX B: SETTLEMENT COMPUTATION

The practically evaluated percentage of change of a representative volume of the clay sample was calculated as follows:

Table B.1 Measured height of 3 marked locations of heated sample

Time (hr)	Measured height			Volume of clay sample
	Point A	Point B	Point C	
0	44163	44862	46078	16623.42
1	44178	44885	46099	16645.73

Therefore the percentage variation of volume = $\frac{16645.73-16623.42}{16645.73}$

= 0.134 %

The percentage change of pore pressure dissipation as predicted by the analytical model was calculated considering the area under the pore pressure variation plot as follows.

Table B.2 Area of pore pressure curve calculations of heated sample

Time (hr)	Area under pore pressure curve (Pa.m)	Area of dissipated pore pressure (Pa.m)
0	397.92	0
1	375.39	22.53

Therefore the percentage variation of area = $\frac{397.92-375.39}{397.92}$

= 0.057 %